EUROTeV-Report-2005-021-1

Dispersion Free Steering and Emittance Tuning Bumps in the ILC Linac

P. Eliasson*, D. Schulte†

November 4, 2005

Abstract

To keep the emittance growth in the ILC main linac at a reasonably low level ($\Delta\epsilon_y < 10$ nm in 90% of all cases), Dispersion Free Steering (DFS) seems to be insufficient. In this report the use of emittance tuning bumps in addition to DFS is investigated. Simulations show that two dispersion bumps may be enough to reduce the emittance growth from 50 nm, after DFS, to approximately 10 nm, as desired. The effect of an additional wakefield bump is also studied giving very good results: an emittance growth of 1.5 nm or less in 90% of all cases. Furthermore, the robustness of the tuning bumps is investigated, showing that the emittance target is reached even in presence of noise during or after the bump tuning.

*CERN, Geneva, Switzerland; Uppsala University, Sweden
†CERN, Geneva, Switzerland

1 Introduction

For the main linac of the future International Linear Collider (ILC) [1] it will be very important to keep the emittance growth $\Delta\epsilon_y$ at a low level. There is not yet an official emittance growth budget for this part of the machine, but in this report a growth of less than 50%, i.e. $\Delta\epsilon_y < 10$ nm, in 90% of all cases is considered a reasonable target.
To reduce emittance growth, beam-based alignment is required. One of the alignment algorithms that has been proposed for the ILC is Dispersion Free Steering (DFS) [2]. However, it is difficult, if not impossible, to reach the target of 10 nm using DFS alone, therefore so-called emittance tuning bumps have to be used as a final stage of correction. In this report two kinds of emittance tuning bumps are discussed: dispersion bumps and wakefield bumps[1].
The implementation of the bumps differs from the one that was previously used for CLIC. The bumps are here tuned to minimise the emittance at the end of the linac instead of directly after each bump. In this way the emittance is tuned at the most relevant position, but at the same time the bumps are no longer independent. Dispersion bumps implemented in this way have already been successfully used as a complement to Ballistic Alignment during ILC simulations [3]. Wakefield bumps using the final emittance as a tuning signal have also been previously studied, but in that case for CLIC [4].
All simulations in this report were performed with the TESLA main linac lattice from the Technical Review Committee (TRC) report [5]. The actual ILC lattice may be slightly different. The main results, except the robustness study, were previously presented in [6].

2 Dispersion Free Steering

One of the beam-based alignment techniques considered for the ILC is so-called Dispersion Free Steering (DFS). During this kind of alignment the main linac is divided into groups (bins) of BPMs and correctors. A nominal beam and one or more help beams with different energies are used to determine the dispersion along the linac. For one bin after the other, the correctors are adjusted, using as low a strength as possible, to minimise the differences between the orbits of the beams. The nominal beam is at the same time steered into the centres of the BPMs. In other words, the aim is to minimise the target function

$$\chi^2 = \sum_{i=1}^{n} \omega_{1,i} y_{0,i}^2 + \sum_{j=1}^{m} \sum_{i=1}^{n} (y_{j,i} - y_{0,i})^2 + \sum_{k=1}^{p} \omega_{2,k} c_k^2 \tag{1}$$

Here, n, m and p are the number of BPMs, help beams and correctors respectively. The offset of beam j (for nominal beam j = 0) in BPM i is denoted $y_{j,i}$, and c_k is the strength of corrector k. In the first and third term, $\omega_{1,i}$ and $\omega_{2,k}$ have been used to denote the DFS weights for orbit and corrector strength. The weights are in this report the same for all BPMs and correctors respectively, i.e. $\omega_{1,i} = \omega_1$, $\omega_{2,k} = \omega_2$, $\forall i, k$.

[1] Observe that the wakefield bumps in this report are not pure wakefield bumps. Because of the way they are designed, they also affect the dispersion, see Section 3.2

Table 1: Beams used for each of the two methods of DFS.

DFS method	Beam 0	Beam 1	Beam 2
gradient-gradient	nominal	10% lower gradient	20% lower gradient
energy-gradient	nominal	20% lower gradient	20% lower energy

Table 2: Optimum weights for orbit and corrector strength (ω_1, ω_2), corresponding average emittance growth $\langle\Delta\epsilon_y\rangle$ and 90th percentile $\Delta\epsilon_y(90\%)$ for 100 machines.

	Gradient-gradient corr. beams				Energy-gradient corr. beams			
	10 μm	5 μm	2 μm	1 μm	10 μm	5 μm	2 μm	1 μm
w_1	0.32	0.32	0.32	0.32	0.040	0.020	0.010	0.010
w_2	0.14	0.14	0.28	0.14	0.018	0.0089	0.0044	0.0044
$\langle\Delta\epsilon_y\rangle$ [nm]	28.2	30.7	29.3	26.5	11.5	8.48	7.82	6.56
$\Delta\epsilon_y(90\%)$ [nm]	54.9	57.0	58.0	54.9	24.7	16.4	16.1	12.2

For the simulations described below, two different ways of varying the energy of the help beams were studied and in both cases three beams were used, see Table 1. For the first method, the different energies are generated by changing the accelerating gradient in the linac. This can easily be done in the ILC. For the second method it is assumed that one of the help beams has a different energy already when entering the linac, even though it is not clear for the moment how to produce this energy difference in reality. Both methods were investigated for four different BPM resolutions: 1, 2, 5 and 10 μm. The optimum DFS weights for orbit and corrector strength were found for each case by scanning 15×15 values, see Table 2. All results were obtained as an average over 100 machines created using the misalignment model developed for the TRC [5]. The result of the scan performed for the gradient-gradient method with a BPM resolution of 10 μm is presented in Figure 1.

For the optimum weights, it is clear that the energy-gradient method is more efficient to reduce the emittance growth, see Figure 2. The difference between the two methods

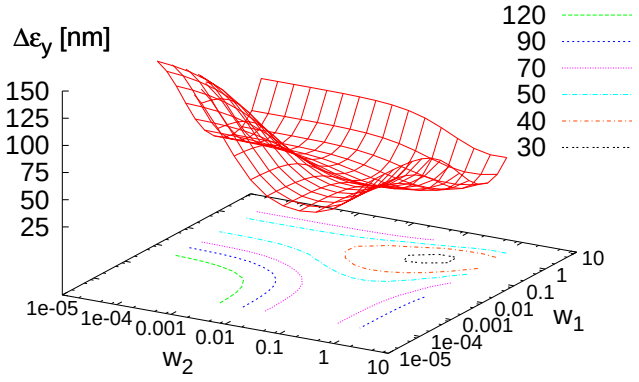

Figure 1: Scan of DFS weights for orbit and corrector strength. Gradient-gradient method, 10 μm BPM resolution.

is even larger for better BPM resolution, cf. Figure 3. These plots also show that the BPM resolution has very little effect on the DFS method using only gradient-gradient modifications, while for the energy-gradient method a good resolution improves the DFS performance. In all cases the emittance growth is still too large after using DFS. Even if 1 μm BPMs were used and a way of performing energy-gradient DFS existed, $\Delta\epsilon_y(90\%)$ would be larger than 12 nm.
Figure 4 shows that much of the total emittance growth in the linac originates from its very first part. This is particularly clear for the gradient-gradient method. One reason is that in the beginning of the linac the gradient change has not yet created a large enough relative energy difference. As a consequence, the differences between the beam trajectories become too small to be accurately measured and the minimisation of Equation. 1 may even contribute to emittance growth. The solution is to give the second term of the target function a lower weight in the beginning of the linac. A second reason for the large initial emittance growth is that early in the linac the energy spread is large and the dispersion is more serious.

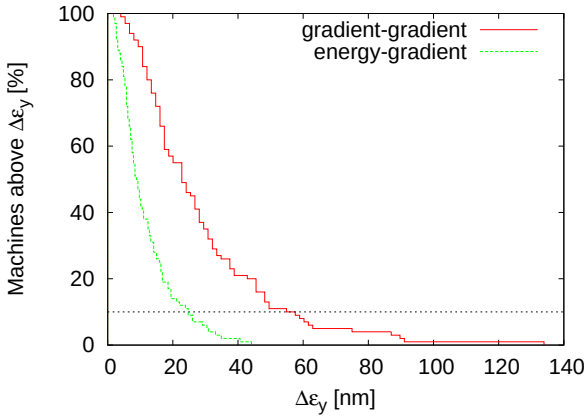

Figure 2: Comparison of the gradient-gradient and the energy-gradient method. BPM resolution = 10 μm.

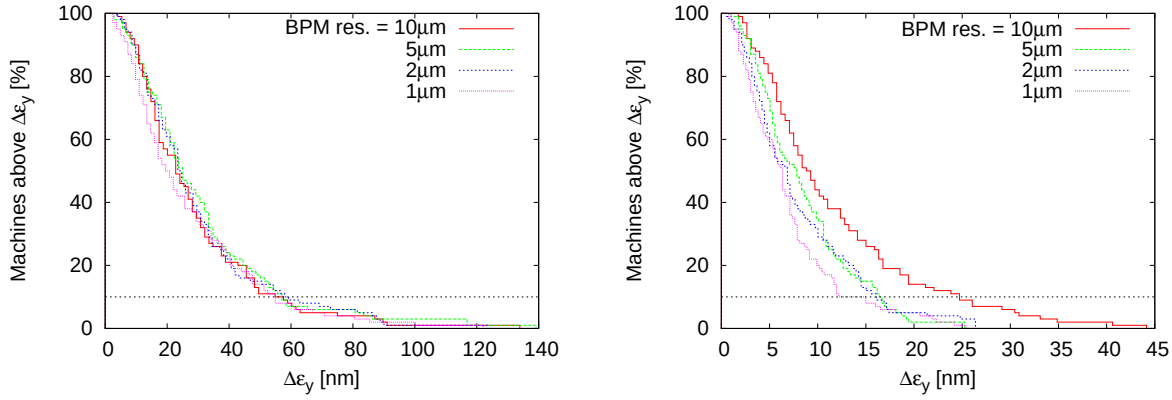

Figure 3: To the left: Gradient-gradient DFS for different BPM resolutions. To the right: Energy-gradient DFS for different BPM resolutions.

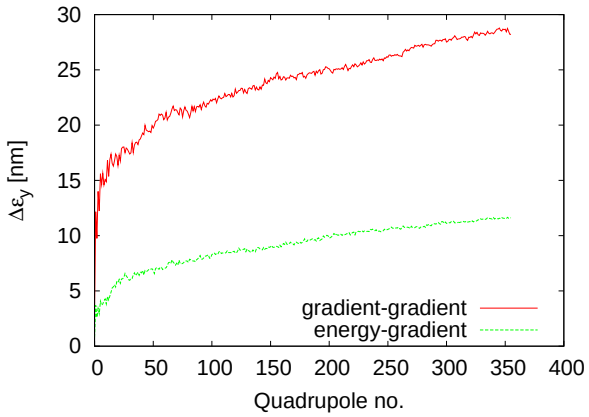

Figure 4: Comparison of the emittance growth along the linac for gradient-gradient and energy-gradient DFS. BPM resolution = 10 μm.

3 Emittance Tuning Bumps

In order to further decrease the emittance growth in the linac, so-called emittance tuning bumps[2] had to be used. During the simulations described below, two types were used: dispersion bumps and wakefield bumps. A conventional dispersion bump is used to generate dispersion at a point along the linac. The emittance is then measured at the nearest downstream measurement station and can be minimised by tuning the generated dispersion. Similarly, a conventional wakefield bump can be tuned to give a wakefield kick that minimises the emittance at the measurement station.
In the simulations below, the bumps were implemented in a slightly different way. Both for the dispersion and the wakefield bumps the tuning was controlled by two knobs acting on different phases. Besides, the measurement station was in both cases positioned at the end of the linac, thereby allowing tuning of the emittance at the most relevant position. The measurement station consisted of two laserwires separated by a betatron phase advance of 90°. Normally, a thin laserwire is used to measure the beam size by scanning. Here, a laserwire with a gaussian transverse profile representing the target beam size was used instead. When the studied beam passes the laserwire its beam profile weighted with the target beam distribution is therefore measured. This "beam-laser luminosity" had in previous studies proven to be a very useful tuning signal both for dispersion bumps and for wakefield bumps [3, 4].
The optimisation of each knob was performed by trying five different knob settings and measuring the beam-laser luminosity at the end of the linac. By fitting a second-order polynomial to the obtained data points a good approximation of the optimal knob setting was achieved. The knobs were optimised one after the other. When all knobs had been optimised the procedure was iterated until convergence.
The first simulations were performed with two and three dispersion bumps respectively. Later simulations also included wakefield bumps.

[2]Based on the idea of the "trajectory bumps" introduced in [7, 8].

3.1 Dispersion Bumps

Each dispersion bump was controlled by two knobs with which the vertical dispersion of offset and angle could be independently adjusted. During the simulations the bumps were simply modeled by changing all particle coordinates by an amount $\Delta y_i = D_y(E_i - E_0)/E_0$ and $\Delta y'_i = D'_y(E_i - E_0)/E_0$ respectively.
One dispersion bump was placed at the beginning and one at the end of the linac. Simulations were later also carried out with a third dispersion bump placed just before the matching section of the linac.
Using only two dispersion bumps, $\Delta\epsilon_y(90\%)$ was decreased to the desired level ($\approx$ 10 nm), both for the gradient-gradient and for the energy-gradient method, see Figure 5. As can be seen the difference between the two methods of DFS is now much less apparent. The effect of having more precise BPMs is also more or less negligible after the dispersion bump optimisation, even for the energy-gradient method, see Figure 6. Further simu-

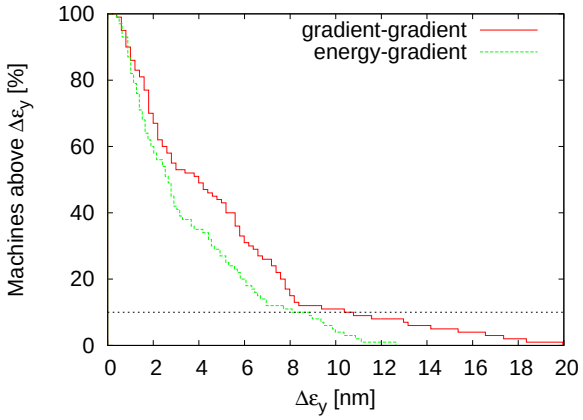

Figure 5: Emittance growth histogram after DFS and optimisation of two dispersion bumps. BPM resolution = 10 μm.

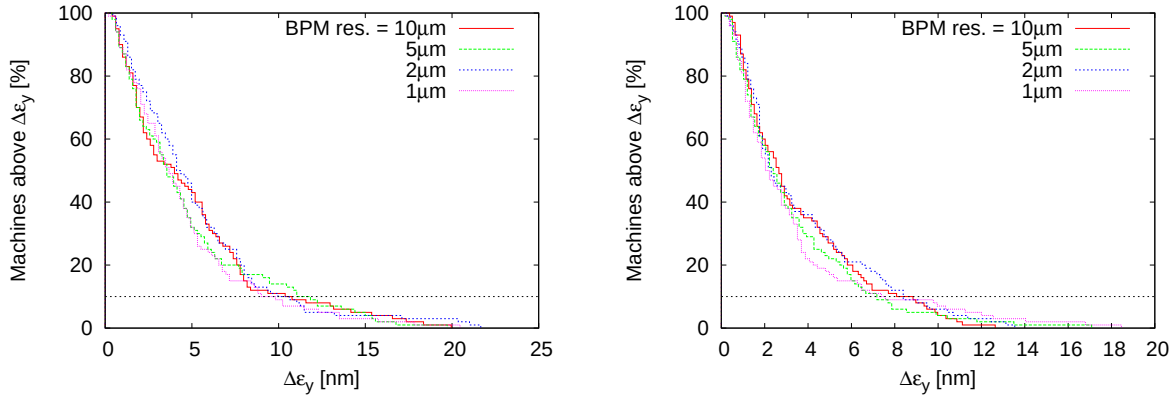

Figure 6: To the left: Gradient-gradient DFS + two dispersion bumps for different BPM resolutions. To the right: Energy-gradient DFS + two dispersion bumps for different BPM resolutions.

lations were carried out with a third dispersion bump just before the matching section of the linac, but this gave no improvement compared to using only two bumps. Instead of increasing the number of dispersion bumps a wakefield bump was added in hope of being able to reduce wakefield induced emittance growth.

3.2 Wakefield Bumps

In order to be able to cancel wakefield kicks from misaligned accelerating structures, a wakefield bump was included in the simulations. This bump consisted of two pairs of quadrupoles. Each pair was controlled by a knob which offset the first quadrupole by an amount Δy and the second by an amount $-\Delta y K_1/K_2$, where K_1 and K_2 are the strength of the first and second quadrupole respectively. The phase advance between the two knobs was a multiple of 360°. In this way the beam is kicked out of its ideal orbit by the first quadrupole and then kicked back by the second. The beam offset in the accelerating structures between the two quadrupoles gives rise to wakefield kicks, and may be adjusted to minimise emittance. The phase advance between the quadrupole pairs is ideally $n \cdot 360° + 90°$. In this case $n \cdot 360° + 60°$, where 60° is the phase advance per FODO cell, was instead chosen.
Since the wakefield bumps were implemented in this way, they also introduce dispersion in the linac. A more proper name may therefore be dispersive wakefield bumps.
In combination with the two dispersion bumps at the beginning and end of the linac, the wakefield bump turned out to be very efficient and $\Delta\epsilon_y(90\%)$ was decreased to less than 6 nm in the case of gradient-gradient DFS, see the left plot of Figure 7. The right plot of this figure shows how much more efficient the extra wakefield bump is than a third dispersion bump. As mentioned above the difference between using the gradient-gradient or the energy-gradient DFS is less apparent after using the dispersion bumps. When a combination of dispersion and wakefield bumps are used, the difference is even smaller, see Figure 8. In Figure 9 the average emittance over the 100 machines is plotted

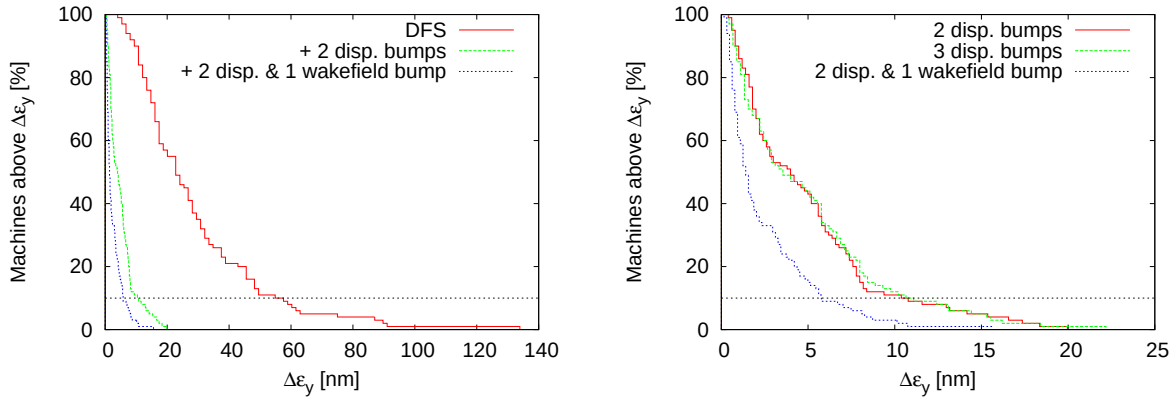

Figure 7: To the left: Emittance growth histogram after gradient-gradient DFS compared to after DFS and optimisation of tuning bumps. To the right: Comparison of different tuning bump configurations.

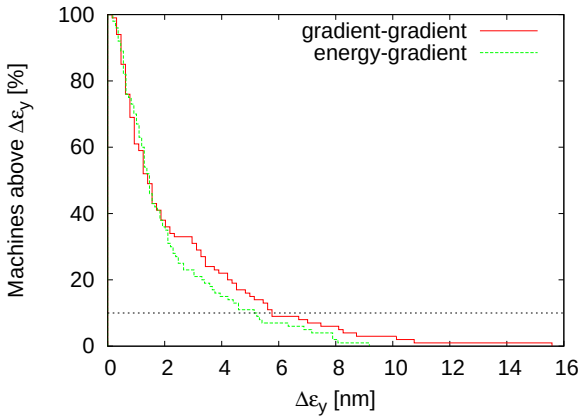

Figure 8: Histogram showing the emittance growth after DFS and optimisation of two dispersion and one wakefield bump. BPM resolution = 10 μm.

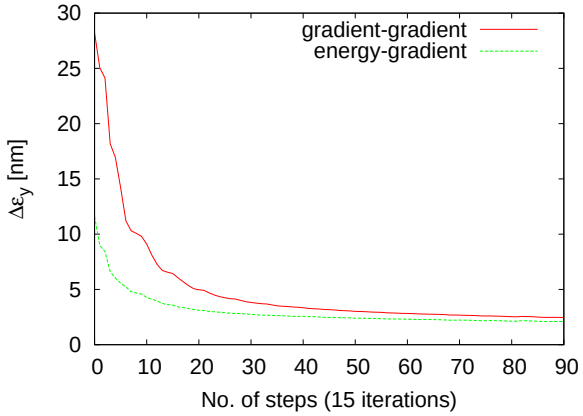

Figure 9: Average emittance growth for 100 machines after each optimisation step. Two dispersion and one wakefield bump were used. DFS with two different methods assuming 10 μm BPM resolution.

for the two DFS methods. This plot shows that even though there is initially a large difference in emittance growth depending on the DFS method used, the difference will quickly decrease when the tuning bumps are optimised. After 90 optimisation steps, the average emittance growth $\langle \Delta\epsilon_y \rangle$ has been reduced to $\approx$ 2 nm, i.e. 10% of the nominal emittance, for the energy-gradient method and slightly more for the gradient-gradient one. The importance of BPM resolution was once again negligible.

3.3 Improved Bump Configuration

The average emittance growth along the linac for the 100 machines is shown for both DFS methods in Figure 10. It is clear that the large initial emittance growth for gradient-gradient DFS can be reduced significantly by placing a dispersion bump at the beginning of the linac. The dispersion bump placed at the end of the linac also seems to be efficient,

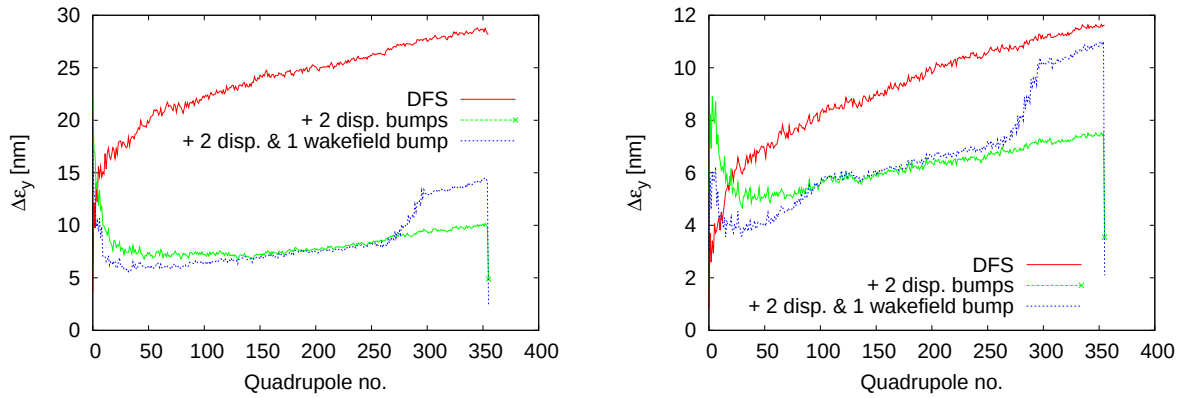

Figure 10: To the left: Average emittance growth (for 100 machines) along the linac. Gradient-gradient DFS alone compared to DFS and tuning bumps. To the right: As in left plot, but with energy-gradient DFS.

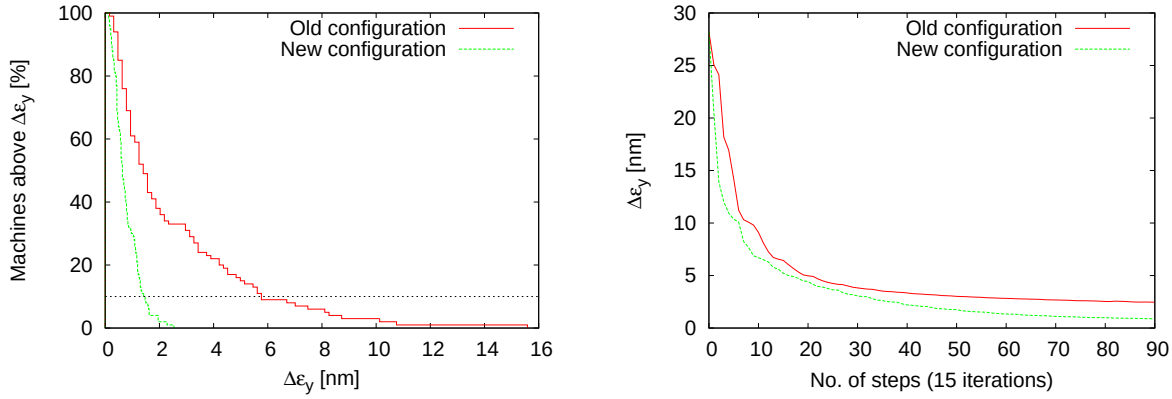

Figure 11: To the left: Comparison of emittance growth histograms for the old and new configuration using two dispersion and one wakefield bump. To the right: Comparison of average emittance growth after each optimisation step for the old and the new bump configuration.

especially when the wakefield bump is also used. This is of course due to the fact that the wakefield bump is not dispersion free, and the final dispersion bump helps by removing this dispersion. In order to avoid that the dispersion created by the wakefield bump reduces its ability to minimise emittance growth, the last dispersion bump was moved to just after the second pair of the wakefield bump. The first quadrupole pair was at the same time moved to the same part of the linac as the second, i.e. between quadrupole no. 250 and 300. This new configuration gave even better results. For the "worst case" (10 μm BPM resolution and gradient-gradient DFS), $\Delta\epsilon_y(90\%)$ was reduced to ≈ 1.5 nm and the average emittance $\langle\Delta\epsilon_y\rangle$ to ≈ 0.76 nm, see Figure 11. By adding another wakefield bump after one third of the linac, immediately followed by a dispersion bump, the emittance could be reduced slightly more: $\Delta\epsilon_y(90\%) \approx 1.4$ nm and $\langle\Delta\epsilon_y\rangle \approx 0.63$ nm. The emittance growth histogram and average emittance along the linac for each of

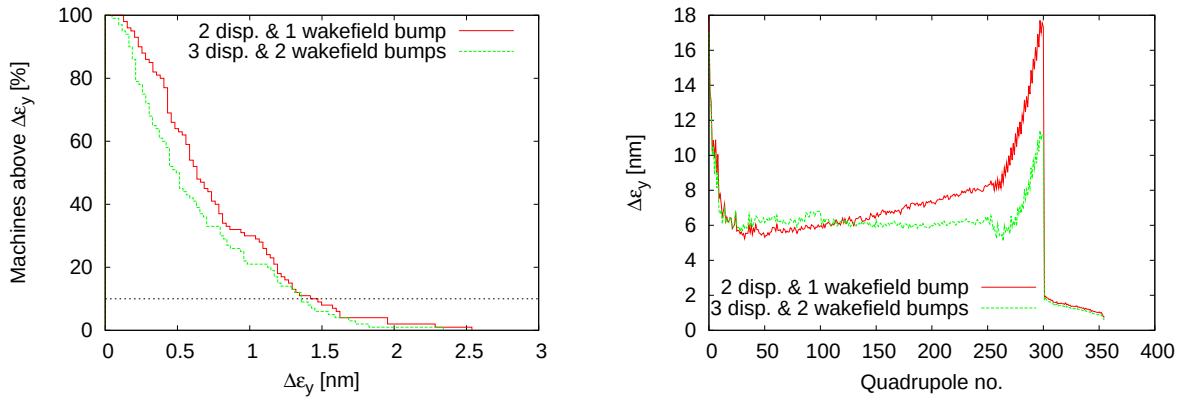

Figure 12: To the left: Emittance growth histogram showing the slight improvement after adding another dispersion and wakefield bump. To the right: Emittance along the linac for the two bump configurations.

these two configurations are shown in Figure 12. Looking at the latter, it is now clear how the wakefield bumps cancel the wakefields in the downstream accelerating structures (especially between quadrupole no. 300 and 355). Even though the difference in final emittance is not large between the two cases, the emittance is more well-behaved in the case with three dispersion and two wakefield bumps.

3.4 Robustness

As has been shown above, the use of dispersion bumps and wakefield bumps as a complement to DFS is very efficient in order to reduce emittance growth. However, in order for the bumps to ultimately be useful, it is important that the tuning bumps work well even in thex presence of noise.

To study the effect of noise on the bump performance, it was assumed that there was an error in the "beam-laser luminosity" measurement with a gaussian distribution ($\sigma = 3\%$, truncated at 3σ). This noise increased the emittance growth from $\Delta\epsilon_y(90\%) \approx 1.4$ nm to $\Delta\epsilon_y(90\%) \approx 4.9$ nm. The additional emittance growth was larger than expected and it was suspected that the optimisation routine used for the perfect case was not optimal for a signal with noise. By slightly modifying the optimisation routine, $\Delta\epsilon_y(90\%)$ was reduced to ≈ 1.8 nm, see Figure 13. In this case the average emittance growth was $\langle\Delta\epsilon_y\rangle \approx 0.94$ nm, compared to $\langle\Delta\epsilon_y\rangle \approx 0.63$ nm for the case without noise. The average final beam-laser luminosity was $\approx 0.2\%$ lower than for a perfect signal. This "luminosity" loss is even less significant than what was observed for CLIC using the same error [4].

Five tests were then carried out to investigate the stability of the final states of the machines: sensitivity to beam jitter; bunch charge and bunch length changes; RF gradient and RF phase variation. For each of these tests, 100 bunches were injected into each of the 100 machines that were obtained after DFS (gradient-gradient method, 10 μm BPMs) and optimised tuning bumps (three dispersion and two wakefield, assuming exact beam-laser luminosity measurement). During the first test the 100 bunches were

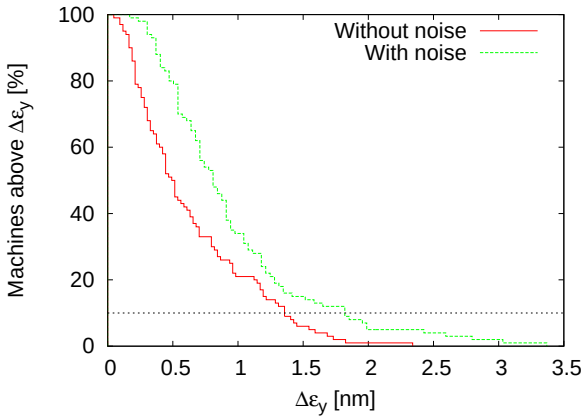

Figure 13: Comparison of emittance growth for bump tuning with and without noise. The noise had a gaussian distribution with $\sigma = 3\%$.

assumed to have an initial vertical offset following a gaussian distribution with standard deviation σ, truncated at 3σ. The average and projected emittance for the 100 bunches at the end of the linac were calculated and averaged over the 100 machines. The beam jitter tolerance was then established by finding the σ that yielded an average projected emittance of 21.63 nm, i.e. 1 nm higher than the emittance for perfect bunches. The corresponding procedure was used for each of the other tests, see the results in Table 3. Observe that for bunch charge and bunch length even the very large variation of $\sigma = 10\%$ hardly changed the emittance and it was no use finding 1 nm tolerances in these cases.

Table 3: Robustness of the tuning bump configuration using three dispersion and two wakefield bumps. For perfect bunches the emittance at the end of the linac was $\epsilon = 20.63$ nm.

Noise source	RMS noise	Average ϵ [nm]	Average projected ϵ [nm]
beam jitter	2.36 μm = $0.222\sigma_y$	20.87	21.63
bunch charge	10%	20.67	20.73
gradient	0.0734%	20.70	21.63
bunch length	10%	20.66	20.67
phase	0.378°	20.68	21.63

4 Conclusion

The use of straightforward DFS alone to minimise emittance growth in the ILC linac seems to be insufficient. The remaining emittance growth after DFS, using the gradient-gradient method and 10 μm BPMs, is $\Delta\epsilon_y(90\%) \approx 50$ nm, which is far above the target ($\Delta\epsilon_y(90\%) < 10$ nm). By using a dispersion bump at the beginning and at the end of the linac, $\Delta\epsilon_y(90\%)$ was reduced to ≈ 10 nm. The use of a third dispersion bump showed no

further improvement. By adding a wakefield bump instead, it was possible to reduce the emittance growth to $\Delta\epsilon_y(90\%) \approx 1.5$ nm. By using three dispersion and two wakefield bumps, $\Delta\epsilon_y(90\%)$ could be reduced to ≈ 1.4 nm and $\langle\Delta\epsilon_y\rangle$ to ≈ 0.63 nm. In this case the emittance along the linac was also more well-behaved. For the most efficient tuning bump configurations the final emittance growth was in principle independent of DFS method and BPM resolution.
The use of a wide laserwire to measure "beam-laser luminosity" proved to work well once again. When taking into account a 3% RMS error in this luminosity signal, $\Delta\epsilon_y(90\%)$ increased to ≈ 1.8 nm and the final luminosity signal was decreased by $\approx 0.2\%$. The stability of the final states of the machines was also tested, with good results. In their final states, the machines are almost completely insensitive to bunch charge and bunch length changes. Tolerances were calculated for beam jitter, RF gradient and RF phase variations.

Acknowledgement

This work is supported by the Commission of the European Communities under the 6^{th} Framework Programme "Structuring the European Research Area", contract number RIDS-011899.

References

[1] ILC homepage, `http://www.linearcollider.org`

[2] T. Raubenheimer, R. D. Ruth, "A Dispersion Free Trajectory Correction Technique for Linear Colliders", Nucl. Instrum. Meth., A302:191-208, 1991

[3] P. Eliasson, D. Schulte, "Simulations of Emittance and Luminosity Tuning Bumps", ILC European Regional Meeting and ILC-BDIR, London, 2005. Available at `https://ilcsupport.desy.de/cdsagenda/fullAgenda.php?ida=a0522`

[4] P. Eliasson, D. Schulte, "Luminosity Tuning Bumps in the CLIC Main Linac", CERN-AB-2005-046, 2005

[5] "ILC-TRC Second Report", SLAC-R-606, 2003

[6] D. Schulte, A. Latina, P. Eliasson, "CERN Contribution to Main Linac Studies", ALCPG and ILC Snowmass Workshop, Snowmass, 2005. Available at `http://alcpg2005.colorado.edu:8080/alcpg2005/program/accelerator/WG1`

[7] J. T. Seeman, F.-J. Decker, I. Hsu, "The Introduction of Trajectory Oscillations to Reduce Emittance Growth in the SLC Linac", SLAC-PUB-5705, 1992

[8] C. Adolphsen, F.-J. Decker, J. T. Seeman, "Flat Beam Studies in the SLC Linac", SLAC-PUB-6255, 1993